Runx1 deficiency protects against adverse cardiac remodeling following myocardial infarction

Title: Runx1 deficiency protects against adverse cardiac remodeling following myocardial infarction

Manuscript number: CIRCULATIONAHA/2017/028911-AR1

Author(s): Christopher Loughrey, University of Glasgow
Charlotte McCarroll, University of Glasgow
Weihong He, University of Glasgow
Kirsty Foote, University of Cambridge
Ashley Bradley, University of Glasgow
Karen McGlynn, University of Glasgow
Francesca Vidler, University of Glasgow
Colin Nixon, Cancer Research UK Beatson Institute
Katrin Nather, University of Glasgow
Caroline Fattah, University of Glasgow

Alexandra Riddell, University of Glasgow

Peter Bowman, University of Glasgow

Elspeth Elliott, University of Glasgow

Margaret Bell, University of Glasgow

Catherine Hawksby, University of Glasgow

Scott MacKenzie, University of Glasgow

Liam Morrison, University of Edinburgh

Anne Terry, University of Glasgow

Karen Blyth, Cancer Research UK Beatson Institute

Godfrey Smith, University of Glasgow

Martin McBride, University of Glasgow

Thomas Kubin, Max-Planck-Institute for Heart and Lung Research, Bad Nauheim, Germany

Thomas Braun, Max-Planck-Institute for Heart and Lung Research

Stuart Nicklin, University of Glasgow

Ewan Cameron, University of Glasgow

Runx1 deficiency protects against adverse cardiac remodeling following myocardial infarction

Running title: McCarroll & He *et al.* Runx1 and myocardial infarction

Charlotte S. McCarroll BVMS PhD[1*], Weihong He MD PhD[1*], Kirsty Foote PhD[2], Ashley Bradley MRes[1], Karen Mcglynn PhD[1], Francesca Vidler MRes[1], Colin Nixon[6], Katrin Nather PhD[1], Caroline Fattah PhD[1], Alexandra Riddell Vet MB MRes[1], Peter Bowman MRes[1], Elspeth B. Elliott PhD[1], Margaret Bell[3], Catherine Hawksby[1], Scott M. MacKenzie PhD[1], Liam J. Morrison BVMS PhD[4], Anne Terry BSc[5], Karen Blyth PhD[6], Godfrey L. Smith PhD[1], Martin W. McBride PhD[1], Thomas Kubin PhD[7], Thomas Braun MD PhD[7], Stuart A. Nicklin PhD[1], Ewan R. Cameron BVMS PhD[3], Christopher M. Loughrey BVMS PhD[1]

[*]CSM and WH; joint first authors

[1] Glasgow Cardiovascular Research Centre, Institute of Cardiovascular and Medical Sciences, University of Glasgow, University Place, Glasgow, G12 8TA, UK.

[2] Division of Cardiovascular Medicine, Addenbrooke's Centre for Clinical Investigation, University of Cambridge, Level 6, Addenbrooke's Hospital, Hills Road, Cambridge, CB2 0QQ, UK.

[3] School of Veterinary Medicine, University of Glasgow, Garscube Campus, Bearsden Road, Glasgow, G61 1QH, UK.

[4] Division of Infection and Immunity, The Roslin Institute, University of Edinburgh, Easter Bush, Midlothian, EH25 9RG, UK.

[5] Centre for Virus Research, University of Glasgow, Garscube Campus, Bearsden Road, Glasgow, G61 1QH, UK.

[6] Cancer Research UK Beatson Institute, Switchback Road, Bearsden, Glasgow, G61 1BD, UK.

[7] Cardiac Development and Remodeling, Max-Planck-Institute for Heart and Lung Research, Ludwigstrasse 43, D-61231, Bad Nauheim, Germany.

Corresponding author

Christopher Loughrey

Institute of Cardiovascular and Medical Sciences,

College of Medical, Veterinary and Life Sciences,

Glasgow Cardiovascular Research Centre, University of Glasgow, University Place,

Glasgow, G12 8TA, UK.

Telephone: 0044 141 330 2753

Email: christopher.loughrey@glasgow.ac.uk

Twitter Handle: @chris_loughrey

Word Count: ~~5166~~5198

Subject Codes: Basic Science Research, Calcium Cycling/Excitation–Contraction Coupling, Pathophysiology, Myocardial Infarction, Remodeling.

ABSTRACT

Background: Myocardial infarction (MI) is a leading cause of heart failure and death worldwide. Preservation of contractile function and protection against adverse changes in ventricular architecture (cardiac remodeling) are key factors to limiting progression of this condition to heart failure. Consequently, new therapeutic targets are urgently required to achieve this aim. Expression of the Runx1 transcription factor is increased in adult cardiomyocytes following MI; however, the functional role of Runx1 in the heart is unknown.

Methods: To address this question, we have generated a novel tamoxifen-inducible cardiomyocyte-specific *Runx1*-deficient mouse. Mice were subjected to MI by means of coronary artery ligation. Cardiac remodeling and contractile function were assessed extensively at the whole heart, cardiomyocyte and molecular levels.

Results: *Runx1* deficient mice were protected against adverse cardiac remodeling post-MI, maintaining ventricular wall thickness and contractile function. Furthermore, these mice lacked eccentric hypertrophy and their cardiomyocytes exhibited markedly improved calcium handling. At the mechanistic level, these effects were achieved through increased phosphorylation of phospholamban by PKA and relief of sarcoplasmic reticulum calcium pump (SERCA) inhibition. Enhanced SERCA activity in Runx1 deficient mice increased sarcoplasmic reticulum calcium content and sarcoplasmic reticulum-mediated calcium release, preserving cardiomyocyte contraction post-MI.

Conclusion: Our data identified Runx1 as a novel therapeutic target with translational potential to counteract the effects of adverse cardiac remodeling, thereby improving survival and quality of life among patients with MI.

Key Words: myocardial infarction, myocytes, calcium, sarcoplasmic reticulum, remodeling

CLINICAL PERSPECTIVE

What is new?

- Our study provides new evidence that *Runx1*, a gene intensively studied in the cancer and blood research fields, has a critical role in cardiomyocytes following myocardial infarction (MI).
- We provide conclusive evidence that increased Runx1 expression under pathological conditions leads to decreased cardiac contractile function.
- Experiments performed utilizing a newly generated cardiomyocyte-specific Runx1 deficient mouse reveal that reducing Runx1 function preserves myocardial contractility and prevents adverse cardiac remodeling post-MI.

What are the clinical implications?

- Our mechanistic data robustly demonstrate that Runx1 modulates cardiac sarcoplasmic reticulum (SR) calcium uptake and contractile function.
- Reducing Runx1 function drives increased contractility post-MI, thereby preserving LV systolic function and preventing adverse cardiac remodeling.
- Our study therefore importantly identifies Runx1 as a new target holding major promise for limiting the progression to heart failure among patients with MI by preventing adverse cardiac remodeling.

BACKGROUND

Acute coronary artery blockage leading to prolonged ischemia and subsequent cardiomyocyte death (myocardial infarction; MI) initiates a reparative process in the heart that is associated with the generation of regional infarct tissue composed predominately of fibrillar collagens. The surviving cardiomyocytes undergo eccentric hypertrophy, a process characterized by cardiomyocyte elongation with reduced diameter and impaired calcium handling, in particular decreased sarcoplasmic reticulum (SR)-mediated calcium uptake[1]. These cellular changes are fundamental to adverse cardiac remodeling, which manifests clinically as left ventricular (LV) wall thinning, dilation and reduced contractility[2]. Together with neurohumoral activation, adverse cardiac remodeling post-MI leads to the clinical syndrome of systolic heart failure (HF), which despite optimized medical therapy is associated with extremely high mortality rates[3]. Novel therapeutic strategies to preserve LV contractile function and limit adverse cardiac remodeling are therefore urgently required to treat patients with MI and improve survival rates and quality of life.

The Runx gene family (*RUNX1, RUNX2* and *RUNX3*) encodes DNA-binding α-subunits that partner core binding factor β (CBF β) to form heterodimeric transcription factors[4]. RUNX proteins act as both activators and repressors of target genes in normal development and disease states[4]. To date, most research has focused on the role of *RUNX1* in hematopoiesis owing to the frequent involvement of this gene in leukemic translocations[4]. By contrast, little was known about the role of Runx1 in the heart. This discrepancy is not surprising given that although Runx1 expression is reported in neonatal cardiomyocytes it decreases to minimal levels in adult cardiomyocytes[5, 6]. However, studies have demonstrated that Runx1 is re-activated in cardiomyocytes of the border zone (BZ) region adjacent to the infarct in both patients with MI and experimental animal models[5, 7]. Whether activation of Runx1 in adult cardiomyocytes following MI is simply a marker of myocardial damage or actually plays a role in the progression of adverse cardiac remodeling is currently unknown.

We have now addressed this question by inducing MI in a mouse model where *Runx1* has been specifically excised in cardiomyocytes. We report that these mice were protected against adverse cardiac remodeling following MI, with markedly preserved LV systolic function through improved SR-mediated calcium uptake. Re-activation of Runx1 following MI therefore plays a crucial role in excitation–contraction (EC) coupling and adverse cardiac remodeling and represents a new therapeutic target with the potential to limit progression to heart failure among patients with MI.

METHODS

Detailed methods are provided in the ~~Supplementary~~ Supplemental Material. Requests by researchers to access the data, analytic methods, and study materials for the purposes of reproducing the results or replicating procedures can be made to the corresponding author who manages the information. The care and use of animals was in accordance with the UK Government Animals (Scientific Procedures) Act 1986 (ASPA). All animal procedures were approved by the University of Glasgow ethical review panel and licensed by the Home Office, UK (Project License Number 600/4503).

Coronary artery ligation

Mice aged 10–12 wk (25–30g) underwent thoracotomy and left anterior descending (LAD) coronary artery ligation (permanent/temporary) using standard approaches.

Generation of cardiomyocyte specific Runx1 knock-out mice

Runx1$^{fl/fl}$ mice described previously[8], were crossed with mice expressing tamoxifen-inducible Cre recombinase (*MerCreMe*) under the control of the cardiac specific alpha-myosin heavy chain (*αMHC*)[9] to produce the relevant test and control cohorts (~~Supplementary~~ Supplemental Material). PCR of genomic DNA, RNA isolation, cDNA synthesis, real-time qPCR analysis and immunoblotting are detailed in the ~~Supplementary~~ Supplemental Material.

Cardiac phenotyping

Echocardiography M-mode measurements were performed before and after LAD ligation and pressure–volume (PV) loop measurements recorded as a terminal procedure using the Scisense/Transonic small animal model PV system.

Histology

Quantification of regional areas and infarct size was performed on picrosirius red/triphenyl tetrazolium chloride (TTC) stained histological sections using Image J and Adobe Photoshop. Cardiomyocyte size was assessed by AlexaFluor-594 conjugated wheat germ agglutinin (WGA; Invitrogen, UK) on adjacent sections. RNAscope using probes to specifically identify cardiomyocyte nuclei (pericentriolar material 1; PCM-1) and Runx1 was performed as detailed in the ~~Supplementary~~ Supplemental Material. For each heart, positive (PPIB and POLR2A) and negative controls (bacterial dapB) were run (~~Supplementary~~ Supplemental Material Figure 1).

Calcium measurements

Cardiomyocytes were isolated as previously described[10], loaded with a calcium–sensitive fluorophore (5.0μmol/L Fura-4F AM, Invitrogen) and perfused during field–stimulation (1.0Hz, 2.0ms duration, stimulation voltage set to 1.5 x threshold). The Fura-4F fluorescence ratio (340/380nm excitation) was measured using a spinning wheel spectrophotometer (Cairn Research Ltd.; sampling rate of 5.0kHz) to measure the intra-cardiomyocyte $[Ca^{2+}]_i$. Cell-edge detection (IonOptix) was used to measure cell length. Data were analyzed offline as previously described[11]. Particular experiments utilized pretreatment (30min) and perfusion with the PKA inhibitor H89 (1μmol/L; Tocris Biosciences, Bristol UK) as previously described[12].

Adenoviral overexpression of *Runx1 in vitro*

Adenoviral vectors expressing either enhanced green fluorescent protein (GFP; Ad-GFP) or GFP and Runx1 in a bicistronic configuration (Ad-Runx1) were prepared and titered (see ~~Supplementary~~ Supplemental Material). Cardiomyocytes isolated from adult New Zealand white rabbits (3kg) were cultured and transduced at a multiplicity of infection (MOI) of 100 for 24h.

Statistics

Data were expressed as mean±SEM. Comparisons between MI and sham hearts were performed using the Student's *t* test on raw data before normalization to percentage change. Comparisons between more than two groups were conducted on raw data using ANOVA. In cases where the two control groups were combined, statistics were performed on the pooled raw data of both control groups and compared with *Runx1*$^{\Delta/\Delta}$ mice using the Student's *t* test. In experiments where multiple isolated cardiomyocyte observations (*n*) were obtained from each heart (*N*), we have firstly ensured normality of data distribution and then determined the differences between control and experimental mice using linear mixed modeling (IBM SPSS Statistics v22) as previously published[13].

RESULTS

Expression of Runx1 following MI

Whilst Runx1 expression has previously been shown to increase at 3 wk post-MI it was unknown whether increased Runx1 expression occurred at a later time-point post-MI (e.g. 8 wk post MI). Furthermore, temporal changes in regional Runx1 expression have not previously been investigated. Runx1 expression was therefore quantified in hearts taken from C57BL/6J mice with MI induced by permanent coronary artery ligation and compared with C57BL/6J mice that had a sham procedure but no coronary artery ligation. PV loop measurements confirmed C57BL/6J mice with MI had reduced systolic (Supplemental Material Figure 2A-C) and diastolic function (Supplemental Material Figure 2D&E) with a lower ejection fraction (Supplemental Material Figure 2F-H).

Runx1 mRNA and protein levels

The levels of *Runx1* mRNA increased by 2.5 fold in whole hearts 4 wk post-MI relative to 4 wk sham hearts ($P<0.05$; Supplemental Material Figure 2I). To determine the contribution of specific myocardial regions to the observed increase in *Runx1* mRNA level, a separate cohort of sham and MI hearts were isolated and tissue isolated from four different regions (Supplemental Material Figure 2J). *Runx1* mRNA levels analyzed using the relative quantification (RQ) method increased by 5.1 fold and 1.8 fold in the infarct (INF) and BZ regions of 4 wk post-MI hearts relative to the respective right ventricular (RV) region ($P<0.05$; Supplemental Material Figure 2K). No detectable change was noted in the *Runx1* mRNA levels in the LV region at 4 wk post-MI and no statistically significant regional differences were detected in the sham hearts (Supplemental Material Figure 2K).

The levels of Runx1 protein changed in line with levels of *Runx1* mRNA (Supplemental Material Figure 2L and M). Runx1 protein levels increased by 6.4 fold and 13.0 fold in the BZ and INF regions, respectively, relative to the LV region in 3 wk post-MI hearts ($P<0.05$).

The pattern of *Runx1* mRNA expression was similar in 8 wk post-MI hearts, with an increase of 3.7 fold and 2.2 fold in the INF and BZ regions, respectively, relative to the corresponding RV region ($P<0.05$; Supplemental Material Figure 3). However, in contrast to 4 wk post-MI hearts, the *Runx1* mRNA levels were increased by 2.7 fold in the LV region relative to the RV region ($P<0.05$) at the 8 wk time point (Supplemental Material Figure 3).
All of the observed regional changes in *Runx1* mRNA expression occurred in the absence of any such changes in the RV region of MI hearts relative to sham hearts.

Expression of Runx1 in cardiomyocytes following MI

We next delineated the spatial-temporal expression of *Runx1* in cardiomyocytes from other cardiac cell types within different regions of the heart using RNAscope. Runx1 expression was found in 8-13% of cardiomyocytes and 5-7% of non-cardiomyocytes in the four regions (RV, LV and equivalent BZ and INF) of sham hearts (Figure 1A, B and C). Runx1 expression did not significantly differ from sham levels in the RV and LV regions at 1 and 14 day post-MI (Figure 1A, B and C). However, Runx1 expression significantly increased to 43% and 44% of cardiomyocytes within the BZ and INF region respectively at 1 day post MI; a time where whole heart contractile dysfunction was also first observed (Figure 1A and B and Supplemental Material Figure 4). Furthermore, Runx1 expression significantly increased to 59% and 47% of cardiomyocytes within the BZ and INF region respectively at 14 day post MI (Figure 1A and B). With regards to other cardiac cell types, Runx1 expression significantly increased to 14% of non-cardiomyocytes within the INF region at 1 day post MI (Figure 1A and C) and increased further to 35% and 26% of non-cardiomyocytes within the BZ and INF region respectively at 14 day post MI (Figure 1A and C). These data supported separate experiments which found an increased *Runx1* level at 1 and 14 days post-MI in cardiomyocytes isolated from whole hearts and separated from other cell types as measured using rtqPCR data even though these data did not provide spatial resolution (Figure 1D).

Direct assessment of *Runx1* function in cardiomyocytes.

To directly determine the contribution of Runx1 in cardiomyocytes to reduced cardiac function, we generated cardiomyocyte-specific *Runx1*-deficient mice using Cre-LoxP-based gene targeting strategies (Supplemental Material and ~~Supplementary~~ Supplemental Material Figure 5)[9]. Three groups of mice were generated: $Runx1^{\Delta/\Delta}$ mice (*αMHC-MerCreMer:*$Runx1^{fl/fl}$); litter-mate $Runx1^{fl/fl}$ mice controlling for the insertion of the LoxP sites[8] and $Runx1^{wt/wt}$ mice controlling for insertion of the tamoxifen-inducible *Cre* recombinase (*αMHC-MerCreMer:*$Runx1^{wt/wt}$)[9]. Cardiomyocyte-specific excision of *Runx1* was induced in adult mice by a single i.p. injection of tamoxifen (40mg/Kg). PCR of genomic DNA, rtqPCR and western blot analysis was performed on isolated cardiomyocytes and confirmed successful deletion of the *Runx1* gene following injection with tamoxifen (~~Supplementary~~ Supplemental Material Figure 5).

***In vivo* echocardiographic assessment of $Runx1^{\Delta/\Delta}$ mice post-MI**

In order to establish whether LV systolic function was altered in $Runx1^{\Delta/\Delta}$ mice post-MI we utilized M-mode echocardiography.

Cardiac function

MI was surgically induced in $Runx1^{\Delta/\Delta}$, $Runx1^{fl/fl}$ and $Runx1^{wt/wt}$ mice 1 wk after tamoxifen injection to all mice. Echocardiography was performed before MI and every 2 wk post-MI to assess cardiac contractile function (Figure 2A). As expected, cardiac systolic function (assessed by fractional shortening) decreased in both groups of control mice ($Runx1^{fl/fl}$ and $Runx1^{wt/wt}$) post-MI (Figure 2B). By contrast, $Runx1^{\Delta/\Delta}$ mice demonstrated a markedly preserved fractional shortening that was 158% of the control mice at 8 wk post-MI (39.5±0.7 vs. 24.9±1.9%; $P<0.05$; Figure 2A and B). $Runx1^{\Delta/\Delta}$ mice undergoing a sham procedure 1 wk post-tamoxifen injection demonstrated no change in fractional shortening over the equivalent 8 wk time course and were not significantly different from the $Runx1^{\Delta/\Delta}$ MI mice

until the 8 wk time point (Figure 2B). The improved fractional shortening in *Runx1*$^{\Delta/\Delta}$ mice post-MI was the culmination of substantially improved cardiac contraction as evidenced by the smaller LV internal diameter measured at systole (LVIDs; Figure 2A and C), which was 77% of the two control groups post-MI (2.5±0.2 vs. 3.3±0.1mm; P<0.05). *Runx1*$^{\Delta/\Delta}$ mice undergoing a sham procedure post-tamoxifen administration demonstrated no change in LVIDs over the equivalent 8 wk time course. The LVID measured at diastole (LVIDd) within the BZ region indicated that the hearts of both control and *Runx1*$^{\Delta/\Delta}$ mice post-MI dilated at this level of the myocardium albeit to a lesser degree in *Runx1*$^{\Delta/\Delta}$ mice (Figure 2D).

Cardiac structure

As expected, LV posterior wall thickness during systole (LVPWs) measured at the level of the BZ of control mice (*Runx1*$^{fl/fl}$ and *Runx1*$^{wt/wt}$) thinned after the 2 wk post-MI time point due to the cardiac remodeling process (Figure 2E). By contrast, *Runx1*$^{\Delta/\Delta}$ mice displayed preserved wall thickness that was 164% of control mice (*Runx1*$^{fl/fl}$ and *Runx1*$^{wt/wt}$) at 8 wk post-MI (2.07±0.14 vs. 1.27±0.06mm; P<0.05; Figure 2E). *Runx1*$^{\Delta/\Delta}$ mice undergoing a sham procedure post-MI demonstrated no change in LVPWs over the equivalent 8 wk time course. The wall-thickness data were confirmed at diastole 8 wk post-MI (Figure 2F).

These data were confirmed in: (i) a separate blinded study (~~Supplementary~~ Supplemental Material Figure 6A-E) where the operator was blinded to the animals undergoing surgery, echocardiography and analysis before MI and at 2 wk post-MI and (ii) at earlier time points at and before 1 wk post-MI (~~Supplementary~~ Supplemental Material Figure 7).

***In vivo* ventricular luminal volumes and ejection fraction in *Runx1*$^{\Delta/\Delta}$ mice 2 wk post-MI**

LV ventricular luminal volume of the *Runx1*$^{\Delta/\Delta}$ and control mice was assessed *in vivo* at 2 wk post-MI using pressure volume (PV) loops (Figure 2G). The end diastolic volume (EDV) in the *Runx1*$^{\Delta/\Delta}$ mice was reduced to 82% of that in the control mice (*Runx1*$^{fl/fl}$ and *Runx1*$^{wt/wt}$), indicating a reduction in LV dilation (36.3±3.00 vs. 44.5±2.47μL; P<0.05; Figure 2G and H).

The end systolic volume (ESV) in *Runx1*$^{\Delta/\Delta}$ mice was reduced to 54% of that of the control mice, indicating a greater level of emptying of LV blood volume (12.9±2.98 vs. 23.7±2.51μL; *P*<0.05; Figure 2G and I). This leftward shift in the PV loop in the *Runx1*$^{\Delta/\Delta}$ mice resulted in an ejection fraction (EF) that was 138% of the control mice (66.3±5.69 vs. 48.0%±3.18%; *P*<0.05; Figure 2G and J).

Histological assessment of *Runx1*$^{\Delta/\Delta}$ mice 8 wk post-MI

Heart structure

We next investigated whether altered whole heart structure contributed to the preserved cardiac performance of *Runx1*$^{\Delta/\Delta}$ mice post-MI. Analysis of the different regions of the heart (Figure 3A) using picrosirius red staining of serial sections of hearts from *Runx1*$^{\Delta/\Delta}$ mice 8 wk post-MI showed that the mean two-dimensional whole heart area (RV+SEP+LV+INF) was 112% of control mice (*Runx1*$^{fl/fl}$ and *Runx1*$^{wt/wt}$) post-MI (37.4±1.4 vs. 33.5±0.6mm^2; *P*<0.05; Figure 3B). This increase in heart area was associated with the LV free wall (Figure 3A; dotted area), which in *Runx1*$^{\Delta/\Delta}$ mice post-MI was 127% of the control mice post-MI (11.0±0.8 vs. 8.7±0.4mm^2; *P*<0.05; Figure 3C). No change was detected in the RV wall area in *Runx1*$^{\Delta/\Delta}$ mice post-MI (Figure 3D) and therefore further investigation focused on the structure of the LV.

LV wall thickness (measured at the level of the BZ; Figure 3A; arrows) in *Runx1*$^{\Delta/\Delta}$ mice post-MI was 127% of control mice post-MI (2.07±0.2 vs. 1.63±0.1mm; *P*<0.05; Figure 3E), a finding that supported the echocardiographic data (Figure 2E). No change was detected in the septal-wall thickness in *Runx1*$^{\Delta/\Delta}$ mice post-MI (Figure 3F) or overall heart weight (Figure 3G). Infarct thickness and fibrosis (Figure 3H&I) was not different in *Runx1*$^{\Delta/\Delta}$ mice post-MI versus control mice post-MI. Furthermore, infarct size (32.3±1.5% *vs.* 32.7±3.1 *vs.* 31.9±5% of LV; Runx1$^{\Delta/\Delta}$ (N=5) *vs.* Runx1$^{wt/wt}$ (N=7) *vs.* Runx1$^{fl/fl}$ (N=5); P>0.05; Figure 3J) at 8 wks post-MI (and the earlier time point of 24 h post-MI; ~~Supplementary~~ Supplemental Material

Figure 8A and B) was not different in *Runx1*$^{\Delta/\Delta}$ versus control mice, and therefore did not explain the preserved LV function observed *in vivo* (Figure 2B).

Cardiomyocyte size

To investigate why LV free wall thickness was preserved in *Runx1*$^{\Delta/\Delta}$ mice 8 wk post MI relative to the wall thinning observed in control mice post-MI (Figures 2E and F), the cardiomyocyte size in *Runx1*$^{\Delta/\Delta}$ mice 8 wk post MI was determined using wheat germ agglutinin staining (WGA). As expected, LV cardiomyocytes from control *Runx1*$^{fl/fl}$ and *Runx1*$^{wt/wt}$ mice 8 wk post-MI exhibited significant cell lengthening to 121% and 118% of *Runx1*$^{\Delta/\Delta}$ sham mice (111.7±3.8 vs. 108.8±3.7 vs. 92.53±1.04μm; $P<0.05$; Figure 3K and L). However, cardiomyocyte elongation was absent in *Runx1*$^{\Delta/\Delta}$ mice at 8 wk post-MI (Figure 3K and L). An equivalent absence of cardiomyocyte lengthening was also observed in septal cardiomyocytes (Figure 3M). LV cardiomyocytes from control *Runx1*$^{fl/fl}$ and *Runx1*$^{wt/wt}$ mice 8 wk post-MI exhibited a significant decrease in cell diameter to 86% and 85% of *Runx1*$^{\Delta/\Delta}$ sham mice (15.91±0.83 vs. 15.88±0.75 vs. 18.86±0.37μm; $P<0.05$; Figure 3N and O). However, cardiomyocyte cell diameter did not decrease in *Runx1*$^{\Delta/\Delta}$ mice 8 wk post-MI (Figure 3O). LV cardiomyocytes from control *Runx1*$^{fl/fl}$ and *Runx1*$^{wt/wt}$ mice 8 wk post-MI exhibited a significant decrease in cardiomyocyte cross-sectional area to 79% and 76% of *Runx1*$^{\Delta/\Delta}$ sham mice (350.6±23.9 vs. 338.2±22.6 vs. 440.0±11.5μm; $P<0.05$; Figure 3N and P). However, cardiomyocyte cell cross-sectional area did not decrease in *Runx1*$^{\Delta/\Delta}$ mice 8 wk post-MI (Figure 3P). No change in septal cardiomyocyte diameter was observed at 8 wk post-MI in any group (Figure 3Q).

Calcium transients in *Runx1*$^{\Delta/\Delta}$ mice 2 wk post-MI

Although increased fractional shortening paralleled increased wall thickness in *Runx1*$^{\Delta/\Delta}$ mice at 8 wk post-MI (Figure 2B and E), we noted that wall thickness was not significantly different between the three groups at 2 wk post-MI. However, *Runx1*$^{\Delta/\Delta}$ mice still exhibited

greater fractional shortening at this time point than was observed for the two control groups. To investigate this dichotomy, we isolated cardiomyocytes from hearts at 2 wk post-MI to characterize calcium handling. This was achieved by measuring the intracellular calcium concentration ($[Ca^{2+}]_i$), focusing on electrically induced SR-mediated calcium release (calcium transients) into the cytosol, which predominately determines the force of contraction.

Cardiomyocytes isolated at 2 wk post-MI were stimulated at 1.0 Hz to elicit calcium transients and cell shortening (Figure 4A-C). The calcium transient peak (systolic $[Ca^{2+}]_i$) in *Runx1*$^{\Delta/\Delta}$ mice was 117% and 122% of the control (*Runx1*$^{fl/fl}$ and *Runx1*$^{wt/wt}$) mice (582.8±36.1 vs. 497.4±31.3 nM vs. 477.0±24.5nM $[Ca^{2+}]_i$; $P<0.05$; Figure 4B and D). The calcium transient minimum (diastolic $[Ca^{2+}]_i$) in *Runx1*$^{\Delta/\Delta}$ mice was 92% and 89% of the control (*Runx1*$^{fl/fl}$ and *Runx1*$^{wt/wt}$) mice (137.8±4.5 vs. 149.8±6.3 vs. 155.1±6.8nM $[Ca^{2+}]_i$; $P<0.05$; Figure 4B and E). The changes in peak and minimum $[Ca^{2+}]_i$ of *Runx1*$^{\Delta/\Delta}$ mice resulted in a calcium transient amplitude which was 128% and 138% of the control (*Runx1*$^{fl/fl}$ and *Runx1*$^{wt/wt}$) mice (445.0±34.3 vs. 347.5±29.0 vs. 321.9±20.7nM $[Ca^{2+}]_i$; $P<0.05$; Figure 4B and F). Furthermore, the time constant of calcium transient decay in the *Runx1*$^{\Delta/\Delta}$ mice was 65% and 55% of the control (*Runx1*$^{fl/fl}$ and *Runx1*$^{wt/wt}$) mice (0.074±0.007 vs. 0.114±0.018 vs. 0.134±0.020s; $P<0.05$; Figure 4B and G), suggesting an increased rate of removal of calcium from the cytosol.

The increased calcium transient amplitude in *Runx1*$^{\Delta/\Delta}$ mice post-MI occurred in the absence of any significant changes in calcium entry or action potential duration (as measured indirectly using the QT interval on the electrocardiogram or directly using voltage measurements on isolated cardiomyocytes at 2 wk post-MI) (~~Supplementary~~ Supplemental Material Figure 9).

Caffeine-induced calcium transients and cell shortening

We hypothesized that the lowered time constant of decay detected in the *Runx1*$^{\Delta/\Delta}$ mice 2 wk post-MI might reflect either increased SR calcium uptake *via* SERCA or extrusion from the cell *via* the sodium calcium exchanger (NCX). To address this issue, we applied a rapid bolus of 10mM caffeine at the end of the protocol to release all of the calcium from the SR into the cytosol. This approach enabled assessment of SR calcium content.

The SR calcium content of the *Runx1*$^{\Delta/\Delta}$ mice was 135% and 118% of the control *Runx1*$^{fl/fl}$ and *Runx1*$^{wt/wt}$ mice, respectively (842.8±47.2 vs. 624.3±42.2 vs. 712.6±40.0nM $[Ca^{2+}]_i$; P<0.05; Figure 4H). SERCA-mediated calcium uptake is bypassed during application of 10mM caffeine and cytosolic calcium removal occurs predominately *via* NCX. The activity of NCX, as assessed by the time constant of caffeine-induced calcium transient decay, was not different between the three groups (Figure 4I).

The increased SR calcium content observed in *Runx1*$^{\Delta/\Delta}$ mice might reflect enhanced SERCA activity (K_{SERCA}). Therefore, we measured the rate constant of decay of the caffeine-induced calcium transient (which includes sarcolemmal efflux but not SR calcium uptake) and subtracted this value from that of the electrically stimulated calcium transient (which includes both SR calcium uptake and sarcolemmal efflux)[14, 15]. The K_{SERCA} of the *Runx1*$^{\Delta/\Delta}$ mice was 148% and 160% of control *Runx1*$^{fl/fl}$ and *Runx1*$^{wt/wt}$ mice (14.4±1.4 vs. 9.7±1.8 vs. 9.0±1.2s^{-1}; P<0.05; Figure 4J). To corroborate that the increased calcium transient amplitude of *Runx1*$^{\Delta/\Delta}$ mice resulted in increased cell shortening, we performed edge-detection shortening measurements (Figure 4C). Cardiomyocyte shortening in *Runx1*$^{\Delta/\Delta}$ mice 2 wk post-MI was 156% and 203% of the control *Runx1*$^{fl/fl}$ and *Runx1*$^{wt/wt}$ mice (7.5±0.9 vs. 4.8±0.6 vs. 3.7±0.4% of diastolic length; P<0.05; Figure 4C and K).

Effect of overexpressing Runx1 on calcium transient amplitude and SR calcium content in normal cardiomyocytes

To further support the novel link between Runx1 and calcium handling in isolated cardiomyocytes, we performed a gain-of-function study by overexpressing Runx1 *via* adenoviral-mediated gene transfer (Ad-Runx1) in isolated adult cardiomyocytes from normal hearts. The calcium transient amplitude in Ad-Runx1-transduced cardiomyocytes was 53% of cardiomyocytes transduced with the control adenoviral vector expressing green fluorescent protein (Ad-GFP) (70.5±8.3 vs. 133.4±30.7nM $[Ca^{2+}]_i$; $P<0.05$; Figure 4L and M). SR calcium content in cardiomyocytes overexpressing Runx1 was 60% of the control cardiomyocytes (388.8±60.3 vs. 651.8±84.4nM $[Ca^{2+}]_i$; $P<0.05$; Figure 4N).

Expression of calcium handling proteins in *Runx1*$^{\Delta/\Delta}$ mice 2 wk post-MI

To investigate the mechanism by which SERCA activity is increased, we quantified the expression and phosphorylation levels of key calcium handling proteins involved in the control of SERCA-mediated calcium uptake in isolated cardiomyocytes 2 wk post-MI.

Levels of phospholamban (PLB), an inhibitory protein that regulates SERCA activity, were not significantly altered in the *Runx1*$^{\Delta/\Delta}$ mice (Figure 5A and B). By contrast, phosphorylation of PLB (which relieves SERCA inhibition and improves cardiac contractility) at the PKA-target residue Ser16 [P-PLB (Ser16)] was 331% of the control mice (*Runx1*$^{wt/wt}$ and *Runx1*$^{fl/fl}$) (331.2±94.5 vs. 100±35.6% change; $P<0.05$; Figure 5A and C).

Decreased levels of PKC indirectly enable enhanced phosphorylation of PLB and increase cardiac contractility[16]; however, no between-group differences were detected in the levels of PKC (Figure 5D and E). Phosphorylation of PLB at the CaMKII-target residue threonine-17 ([P-PLB (Thr17)] in *Runx1*$^{\Delta/\Delta}$ mice was 175% of the control mice (*Runx1*$^{wt/wt}$ and *Runx1*$^{fl/fl}$) (175.0±22.9 vs. 100±8.2% change; $P<0.05$; Figure 5D and F). A possible regulator of phosphorylation of PLB is protein phosphatase 1 (PP1), which dephosphorylates PLB[16]. We

found that expression of PP1 in *Runx1*$^{\Delta/\Delta}$ mice was decreased to 28% of the control mice (*Runx1*$^{wt/wt}$ and *Runx1*$^{fl/fl}$) post-MI (27.6±19.4 vs. 100±21.3% change; $P<0.05$; Figure 5G and H).

To confirm that the increased SERCA activity, SR calcium content and calcium transient amplitude observed in *Runx1*$^{\Delta/\Delta}$ mice 2 wk post-MI (Figure 4) were PKA-mediated; we investigated the effect of the PKA inhibitor (H89) on calcium handling. Addition of H89 completely blocked enhancement of all three parameters in the *Runx1*$^{\Delta/\Delta}$ mice relative to the control *Runx1*$^{wt/wt}$ and *Runx1*$^{fl/fl}$ mice (Figure 5I–K).

Cardiac contractility in *Runx1*$^{\Delta/\Delta}$ mice after ischemia with reperfusion

Reperfusion of a blocked coronary artery limits cell death following MI; this effect can be achieved clinically *via* percutaneous coronary intervention. We therefore tested whether *Runx1*$^{\Delta/\Delta}$ mice also maintain a preserved LV contractile function in an additional clinically relevant model of ischemia with reperfusion (I/R).

The left anterior descending coronary artery was temporarily ligated *in vivo* for 45min followed by reperfusion and the *Runx1*$^{\Delta/\Delta}$ mice recovered for 8 wk. Fractional shortening was assessed using echocardiography before MI and weekly after the induction of MI with reperfusion. As expected, fractional shortening decreased in control *Runx1*$^{fl/fl}$ mice after reperfusion (Figure 6A and B). By contrast, *Runx1*$^{\Delta/\Delta}$ mice demonstrated markedly preserved fractional shortening, which was 154% of control *Runx1*$^{fl/fl}$ mice at 8 wk post-reperfusion (42.7±1.5 vs. 27.7±2.13%; $P<0.05$; Figure 6A and B). As with the animal model of permanent coronary artery ligation, infarct size at 8 wks post-reperfusion (and the earlier time point of 24 h post-reperfusion) was not different in *Runx1*$^{\Delta/\Delta}$ versus control mice (Figure 6C and Supplemental Material Figure 8C and D).

DISCUSSION

Runx1 has been most intensively studied in the hematopoietic system because its function is frequently corrupted in different subtypes of leukemia. Although it is known to have a role in lineage differentiation and tissue function in a range of other systems there is almost no information relating to its role in adult cardiomyocytes other than the observation that it can be reactivated following myocardial insult[5, 7]. Our novel study addressed a vital question; namely, is increased expression of RUNX1 post-MI merely a marker of ischemic damage or does it play a functional role in adult cardiomyocytes following MI? We provide new evidence that *Runx1* has an important role in cardiomyocytes following MI. Reducing *Runx1* function preserved cardiac contractility and prevented adverse cardiac remodeling, which suggests that targeting the actions of this gene could have important implications for patient survival post-MI. Importantly, this research transcends discipline boundaries as it not only widens the importance of Runx1 to other fields of medicine but also describes a novel function for this gene.

Our results provide the first detailed quantification of regional *Runx1* expression in mouse heart tissue after myocardial infarction. At 4 wk post-MI, *Runx1* mRNA was increased within the BZ myocardium and INF region which was sustained until at least 8 wk post-MI, at which time point *Runx1* expression also increased within the remote LV myocardium. This is important given that changes in Runx1 expression at the mRNA and protein level are not restricted to rodent MI models but also occur in patients with MI[5, 7]. In separate experiments, we were able to demonstrate that *Runx1* expression is increased within the BZ and INF region post-MI within the contractile elements of the heart i.e. the cardiomyocytes, as early as 1 to 14 days post-MI (Figure 1).

To determine the specific contribution of Runx1 in cardiomyocytes to reduced cardiac contractility, we generated a new tamoxifen-inducible cardiomyocyte-specific Runx1 deficient mouse with the hypothesis that these mice would demonstrate improved cardiac

function. Induction of MI in control transgenic mice led to the expected LV wall thinning, cardiac dilation and reduced contractility 8 wk post-MI. However, all of these adverse cardiac remodeling parameters were absent or reduced in *Runx1*$^{\Delta/\Delta}$ mice at this time point. One possible explanation for the observed preservation of systolic function could have been a reduction in the infarct size of *Runx1*$^{\Delta/\Delta}$ mice given that infarct size correlates with systolic function[17]. However, *Runx1*$^{\Delta/\Delta}$ mice exhibited preservation of geometric shape and contractility post-MI, with no difference in infarct size (at both early and late time points) or fibrosis versus the control mice.

To establish the mechanism underlying these notable findings, we first investigated cardiomyocyte size. Control mice demonstrated the expected cardiomyocyte lengthening and thinning (eccentric hypertrophy) at 8 wk post-MI[1]. However, these changes were absent in *Runx1*$^{\Delta/\Delta}$ mice. Such protection against eccentric hypertrophy at 8 wk post-MI seems highly likely to have afforded *Runx1*$^{\Delta/\Delta}$ mice protection from ventricular dilation and thinning, ultimately leading to preserved contractility. Nevertheless, at 2 wk post-MI, the wall thickness in *Runx1*$^{\Delta/\Delta}$ mice was comparable to that of control mice (as wall thinning in control mice had not yet begun) but contractile function was still dramatically improved. This finding indicated that prevention of wall thinning and dilation could not fully explain the preserved contractile function observed at 2 wk post-MI.

The above dichotomy led us to investigate calcium handling in cardiomyocytes isolated from *Runx1*$^{\Delta/\Delta}$ mice 2 wk post-MI, in particular electrically stimulated calcium release (the calcium transient) from the intra-cardiomyocyte calcium store (the SR) and subsequent cell shortening. Patients and animal models with MI typically exhibit calcium transients with lower amplitude and a slower rate of decline than control/healthy cardiomyocytes, an observation largely attributed to reduced SR-mediated calcium uptake *via* SERCA[15]. *Runx1*$^{\Delta/\Delta}$ mice exhibited increased calcium transient amplitude and reduced time constant of decline post-MI compared to control mice post-MI, resulting in an increase in cell shortening. The

accompanying higher SR calcium content observed in *Runx1*$^{\Delta/\Delta}$ mice post-MI can explain the enhanced calcium transient amplitude[18] since equalizing the SR calcium content with H89 resulted in a calcium transient equivalent to control.

Analysis of the caffeine-induced calcium transient found no detectable change in NCX activity in *Runx1*$^{\Delta/\Delta}$ mice post-MI as compared to control mice post-MI. However, enhanced SR-mediated calcium uptake *via* SERCA was observed in the *Runx1*$^{\Delta/\Delta}$ mice. SERCA activity is a major determinant of the SR calcium content. Furthermore, this pump is regulated predominately by the inhibitory protein phospholamban (PLB). Although expression of PLB was not altered in *Runx1*$^{\Delta/\Delta}$ mice post-MI, we explored some of the proteins that regulate PLB activity[16].

PLB-mediated inhibition of SERCA is balanced by phosphorylation by PKA and CaMKII (which relieves SERCA inhibition) and dephosphorylation by PP1 (which returns PLB to its inhibitory state[16]). We found that ventricular cardiomyocytes from *Runx1*$^{\Delta/\Delta}$ mice exhibited increased PKA-mediated phosphorylation of PLB possibly as a result of reduced levels of PP1. These mechanistic data suggest that PLB phosphorylation stimulates SERCA activity in *Runx1*$^{\Delta/\Delta}$ mice post-MI, and leads to an increased SR calcium content, which in turn increases electrically induced SR-mediated calcium release and doubles cardiomyocyte contraction. Our proposed mechanism was supported by complete blockage of the enhanced calcium transient in cardiomyocytes from *Runx1*$^{\Delta/\Delta}$ mice 2 wk post-MI by inhibition of PKA. The enhanced rate of removal of calcium from the cytosol following increased SERCA activity is sufficient to reduce the end diastolic $[Ca^{2+}]_i$, which not only improves whole heart relaxation but may also limit the stimulation of hypertrophic factors[1].

Previous studies strongly support our proposed mechanism that the effect of Runx1 on SR function is a major contributor to the beneficial effects observed in *Runx1*$^{\Delta/\Delta}$ mice post-MI. Decreased SR function has been demonstrated among patients with HF[15] and enhanced

SR-mediated calcium cycling markedly preserved contractility, reduced adverse cardiac remodeling and delayed progression to heart failure at levels not dissimilar from those observed in the current study[16, 19].

The key findings of our study will likely initiate further research into the beneficial effects of decreasing Runx1 expression in alternative animal models of cardiac disease. As testament to this goal, we found that *Runx1*$^{\Delta/\Delta}$ mice are protected from adverse cardiac remodeling in a separate clinically relevant surgical model. In this model, the blocked coronary artery was subsequently unblocked after a period of ischemia, as would be the case for patients undergoing percutaneous coronary intervention. These additional data further support our study and the translational potential of this new target.

Although our strategy did not result in inactivation of the Runx1 gene in all cardiomyocytes, we postulate that cardiac function improves when only a subset of cardiomyocytes benefits from better Ca^{2+} handling after inactivation of Runx1. Since it is more feasible in a clinical setting to suppress genes in a subset of cardiomyocytes rather than in all cells, we think Runx1, or targets showing a similar potency, are particularly attractive for therapeutic interventions.

In conclusion, we have demonstrated for the first time that Runx1 modulates cardiac SR calcium uptake and contractile function. Reducing Runx1 function drives increased contractility post-MI, thereby preserving LV systolic function and preventing adverse cardiac remodeling. Clinical studies clearly demonstrate that preserving cardiac contractility and protecting against adverse cardiac remodeling are key factors to limiting progression from MI to heart failure[2]. Identification of a new therapeutic target that achieves this objective is urgently required. To this end, we envisage that Runx1 will be exploited in future basic and translational studies to limit progression of patients with MI to heart failure, thereby improving survival rates and quality of life.

ACKNOWLEDGMENTS

We would like to thank Leon de Windt (Maastricht University, Netherlands) for the gift of *αMHC-MerCreMer*:*Runx1*$^{wt/wt}$ mice, Nancy Speck (University of Pennsylvania) for the gift of *Runx1*$^{fl/fl}$ mice, ~~Stephano~~ Stefano Stifani (McGill University) for the gift of Ad-Runx1, Jim Neil (University of Glasgow) for contribution to the manuscript, Vicky Heath for editorial assistance, John McClure (University of Glasgow) for statistical advice and technical advice from Alma Jenkins (University of Glasgow, UK), Nancy Mackay (University of Glasgow, UK) and Mark Hughes (Beatson Institute, UK).

FUNDING SOURCES

UK Medical Research Council (MR/M021459/1), British Heart Foundation (PG/09/004), UK Medical Research Council (MR/K501335/1), Cancer Research UK (C596/A17196) and University of Glasgow, UK.

DISCLOSURES

None.

REFERENCES

1. Kehat I and Molkentin JD. Molecular pathways underlying cardiac remodeling during pathophysiological stimulation. *Circulation*. 2010;122:2727-2735.

2. Konstam MA, Kramer DG, Patel AR, Maron MS and Udelson JE. Left ventricular remodeling in heart failure: current concepts in clinical significance and assessment. *JACC Cardiovasc Imaging*. 2011;4:98-108.

3. Roger VL. Epidemiology of heart failure. *Circulation research*Res. 2013;113:646-59.

4. Blyth K, Cameron ER and Neil JC. The RUNX genes: gain or loss of function in cancer. *Nat Rev Cancer*. 2005;5:376-387.

5. Kubin T, Pöling J, Kostin S, Gajawada P, Hein S, Rees W, Wietelmann A, Tanaka M, Lörchner H, Schimanski S, Szibor M, Warnecke H and Braun T. Oncostatin M is a major mediator of cardiomyocyte dedifferentiation and remodeling. *Cell Stem Cell*. 2011;9:420-432.

6. Eulalio A, Mano M, Dal Ferro M, Zentilin L, Sinagra G, Zacchigna S and Giacca M. Functional screening identifies miRNAs inducing cardiac regeneration. *Nature*. 2012;492:376-381.

7. Gattenlohner S, Waller C, Ertl G, Bultmann BD, Muller-Hermelink HK and Marx A. NCAM(CD56) and RUNX1(AML1) are up-regulated in human ischemic cardiomyopathy and a rat model of chronic cardiac ischemia. *Am J Pathol*. 2003;163:1081-1090.

8. Growney JD, Shigematsu H, Li Z, Lee BH, Adelsperger J, Rowan R, Curley DP, Kutok JL, Akashi K, Williams IR, Speck NA and Gilliland DG. Loss of Runx1 perturbs adult hematopoiesis and is associated with a myeloproliferative phenotype. *Blood*. 2005;106:494-504.

9. Sohal DS, Nghiem M, Crackower MA, Witt SA, Kimball TR, Tymitz KM, Penninger JM and Molkentin JD. Temporally regulated and tissue-specific gene manipulations in the adult and embryonic heart using a tamoxifen-inducible Cre protein. *Circulation research*Res. 2001;89:20-25.

10. Loughrey CM, Smith GL and MacEachern KE. Comparison of Ca^{2+} release and uptake characteristics of the sarcoplasmic reticulum in isolated horse and rabbit cardiomyocytes.

American journal J of pPhysiology Heart and cCirculatory physiologyPhysiol. 2004;287:H1149-H1159.

11. Elliott EB, Hasumi H, Otani N, Matsuda T, Matsuda R, Kaneko N, Smith GL and Loughrey CM. K201 (JTV-519) alters the spatiotemporal properties of diastolic Ca^{2+} release and the associated diastolic contraction during beta-adrenergic stimulation in rat ventricular cardiomyocytes. *Basic research Res in cCardiology*. 2011;106:1009-1022.

12. Zhang M, Prosser BL, Bamboye MA, Gondim AN, Santos CX, Martin D, Ghigo A, Perino A, Brewer AC, Ward CW, Hirsch E, Lederer WJ and Shah AM. Contractile Function During Angiotensin-II Activation: Increased Nox2 Activity Modulates Cardiac Calcium Handling via Phospholamban Phosphorylation. *Journal of the American College of Cardiology*. 2015;66:261-272.

13. Clarke JD, Caldwell JL, Horn MA, Bode EF, Richards MA, Hall MC, Graham HK, Briston SJ, Greensmith DJ, Eisner DA, Dibb KM and Trafford AW. Perturbed atrial calcium handling in an ovine model of heart failure: potential roles for reductions in the L-type calcium current. *J ournal of mMolecular and cCell ular cCardiology*. 2015;79:169-179.

14. Diaz ME, Graham HK and Trafford AW. Enhanced sarcolemmal Ca^{2+} efflux reduces sarcoplasmic reticulum Ca^{2+} content and systolic Ca^{2+} in cardiac hypertrophy. *Cardiovascular Research*. 2004;62:538-547.

15. Piacentino V, 3rd, Weber CR, Chen X, Weisser-Thomas J, Margulies KB, Bers DM and Houser SR. Cellular basis of abnormal calcium transients of failing human ventricular myocytes. *Circ Res*. 2003;92:651-658.

16. Haghighi K, Bidwell P and Kranias EG. Phospholamban interactome in cardiac contractility and survival: A new vision of an old friend. *J ournal of mMol ecular and cCell lular cCardiology*. 2014;77:160-167.

17. Takagawa J, Zhang Y, Wong ML, Sievers RE, Kapasi NK, Wang Y, Yeghiazarians Y, Lee RJ, Grossman W and Springer ML. Myocardial infarct size measurement in the mouse chronic infarction model: comparison of area- and length-based approaches. *J Appl Physiol (1985)*. 2007;102:2104-2111.

18. Trafford AW, Diaz ME, Sibbring GC and Eisner DA. Modulation of CICR has no maintained effect on systolic Ca^{2+}: simultaneous measurements of sarcoplasmic reticulum and sarcolemmal Ca^{2+} fluxes in rat ventricular myocytes. ~~*The J*~~*ournal of* ~~*physiology*~~*Physiol*. 2000;522 Pt 2:259-720.

19. Fish KM, Ladage D, Kawase Y, Karakikes I, Jeong D, Ly H, Ishikawa K, Hadri L, Tilemann L, Muller-Ehmsen J, Samulski RJ, Kranias EG and Hajjar RJ. AAV9.I-1c delivered via direct coronary infusion in a porcine model of heart failure improves contractility and mitigates adverse remodeling. *Circ*~~*ulation*~~ *Heart* ~~*failure*~~*Fail*. 2013;6:310-317.

FIGURE LEGENDS

Figure 1. Runx1 expression in WT C57BL/6 mice post-MI. (A) Typical images of regional heart sections with RNA *in situ* hybridization (using RNAscope®). Regions examined were right ventricle (RV), left ventricle (LV), border zone (BZ) and infarct (INF) in 1 day (middle; *n*=3) and 14 day (bottom; *n*=3) post-MI and equivalent regions in sham hearts (top; *n*=5). Probes for Runx1 (pink) and PCM-1 (cardiomyocyte specific; brown) were used; colored punctate dots represent positive staining (arrows). Scale bar (10μm); magnified insert image (5μm). **(B)** Mean quantification of cardiomyocytes (PCM-1+) and **(C)** non-cardiomyocytes PCM-1-) with Runx1 positive staining as a % of the total number of cardiomyocytes or non-cardiomyocytes respectively (**P*<0.05, 1 day post-MI vs. sham; #*P*<0.05, 14 day post-MI vs. sham - Student's t-test). **(D)** Runx1 expression as measured by rtPCR in cardiomyocytes isolated from whole sham (*n*=17) and 1 day (*n*=8), 7 day (*n*=6) and 14 day (*n*=3) post-MI hearts (ANOVA). Stock (C57BL/6J; *n*=4) mice were included to show that there was no detectable difference with sham hearts (ANOVA).

Figure 2. Cardiac function in *Runx1*$^{\Delta/\Delta}$ mice. (A) Echocardiography (scale:x=0.1s;y=2mm). **(B)** 8 wk echocardiographic data for fractional shortening (FS) and **(C)** LV internal diameter (LVID) at systole (LVIDs), **(D)** LVID at diastole (LVIDd), **(E)** LV posterior wall thickness at systole (LVPWs) and **(F)** LVPW thickness at diastole (LVPWd). (*Runx1*$^{fl/fl}$ MI and *Runx1*$^{wt/wt}$ MI combined [*n*=11], *Runx1*$^{\Delta/\Delta}$ MI [*n*=9] and *Runx1*$^{\Delta/\Delta}$ sham [*n*=5]), (ANOVA). #P<0.05=Runx1$^{\Delta/\Delta}$ MI mice versus Runx1$^{\Delta/\Delta}$ sham mice *P<0.05=Runx1$^{\Delta/\Delta}$ MI mice versus control Runx1$^{fl/fl}$ MI and Runx1$^{wt/wt}$ MI mice combined. **(G)** Pressure–volume (PV) loops of *Runx1*$^{wt/wt}$ and *Runx1*$^{\Delta/\Delta}$ 2 wk post-MI. **(H)** Mean PV data 2 wk post-MI End diastolic volume (EDV), **(I)** End systolic volume (ESV) and **(J)** Ejection fraction (EF) (*Runx1*$^{fl/fl}$ MI and *Runx1*$^{wt/wt}$ MI combined [*n*=11], *Runx1*$^{\Delta/\Delta}$ MI [*n*=8]), **P*<0.05 Student's t-test.

Figure 3. *Runx1*$^{\Delta/\Delta}$ mice cardiac structure 8 wk post-MI. (A) Picrosirius red stained hearts (BZ,border zone; LV,left ventricle; INF,infarct; RV,right ventricle; SEP,septum; scale: 1mm). Mean **(B)** area of whole heart (all regions), **(C)** LV, **(D)** RV and **(E)** LV wall thickness at BZ region, **(F)** septum wall thickness at BZ region level, **(G)** heart weight to body weight ratio, **(H)** infarct thickness, **(I)** LV fibrosis and **(J)** infarct size (*Runx1*$^{fl/fl}$ MI and *Runx1*$^{wt/wt}$ MI combined [*n*=12], *Runx1*$^{\Delta/\Delta}$ MI [*n*=5]; **P*<0.05), Student's t-test. **(K)** Wheat germ agglutinin (WGA) staining of LV cardiomyocytes (longitudinal) of *Runx1*$^{fl/fl}$ MI (top) and *Runx1*$^{\Delta/\Delta}$ (bottom) post-MI (scale bar:25mm). **(L)** Mean LV cardiomyocyte length (*Runx1*$^{\Delta/\Delta}$ sham [*n*=55 cardiomyocytes,*n*=3 hearts], *Runx1*$^{fl/fl}$ MI [*n*=122 cardiomyocytes,*n*=6 hearts], *Runx1*$^{wt/wt}$ MI [*n*=109 cardiomyocytes from *n*=6 hearts], *Runx1*$^{\Delta/\Delta}$ MI [*n*=102 cardiomyocytes,*n*=6 hearts]), **P*<0.05 linear mixed modelling. **(M)** Mean SEP cardiomyocyte length (*Runx1*$^{\Delta/\Delta}$ sham [*n*=29 cardiomyocytes,*n*=3 hearts], *Runx1*$^{fl/fl}$ MI [*n*=82 cardiomyocytes,*n*=6 hearts], *Runx1*$^{wt/wt}$ MI [*n*=84 cardiomyocytes,*n*=6 hearts], *Runx1*$^{\Delta/\Delta}$ MI [*n*=64 cardiomyocytes,*n*=6 hearts]. **(N)** WGA staining of LV cardiomyocytes (transverse) of *Runx1*$^{wt/wt}$ MI (Left) and *Runx1*$^{\Delta/\Delta}$ MI (Right) (scale bar:25mm). **(O)** Mean LV cardiomyocyte diameter (*Runx1*$^{\Delta/\Delta}$ sham [*n*=449 cardiomyocytes,*n*=3 hearts), *Runx1*$^{fl/fl}$ MI [*n*=811 cardiomyocytes,*n*=6 hearts], *Runx1*$^{wt/wt}$ MI [*n*=897 cardiomyocytes,*n*=6 hearts], *Runx1*$^{\Delta/\Delta}$ MI [*n*=878 cardiomyocytes,*n*=6 hearts]). **(P)** Mean LV cardiomyocyte cross sectional area (*Runx1*$^{\Delta/\Delta}$ sham [*n*=403 cardiomyocytes,*n*=3 hearts), *Runx1*$^{fl/fl}$ MI [*n*=714 cardiomyocytes,*n*=6 hearts], *Runx1*$^{wt/wt}$ MI [*n*=785 cardiomyocytes,*n*=6 hearts], *Runx1*$^{\Delta/\Delta}$ MI [*n*=699 cardiomyocytes,*n*=6 hearts]). **(Q)** Mean SEP cardiomyocyte diameter (*Runx1*$^{\Delta/\Delta}$ sham [*n*=238 cardiomyocytes,*n*=3 hearts], *Runx1*$^{fl/fl}$ MI [*n*=465 cardiomyocytes,*n*=6 hearts], *Runx1*$^{wt/wt}$ MI [*n*=454 cardiomyocytes,*n*=6 hearts], *Runx1*$^{\Delta/\Delta}$ MI [*n*=452 cardiomyocytes,*n*=6 hearts]), **P*<0.05 linear mixed modelling.

Figure 4. Excitation–contraction coupling in *Runx1*$^{\Delta/\Delta}$ mice 2 wk post-MI. (A) Protocol **(B)** Typical calcium (Ca^{2+}) transients and **(C)** cell shortening. Mean Ca^{2+} transient: **(D)** peak, **(E)** minimum and **(F)** amplitude (*Runx1*$^{fl/fl}$ MI [*n*=25 cardiomyocytes,*n*=3 hearts], *Runx1*$^{wt/wt}$

MI [*n*=28 cardiomyocytes,*n*=4 hearts], *Runx1*$^{\Delta/\Delta}$ MI [*n*=28 cardiomyocytes,*n*=3 hearts]; **P*<0.05 *Runx1*$^{\Delta/\Delta}$ MI vs. *Runx1*$^{fl/fl}$ MI and *Runx1*$^{wt/wt}$ MI combined, linear mixed modelling). **(G)** Mean time constant of Ca^{2+} transient decay. **(H)** Mean caffeine-induced Ca^{2+} transient amplitude. **(I)** Mean time constant of decay for caffeine-induced Ca^{2+} transient amplitude. **(J)** Mean sarco–endoplasmic reticulum calcium transport ATPase (SERCA) activity. **(K)** Mean fractional shortening (*Runx1*$^{fl/fl}$ MI [*n*=27 cardiomyocytes,*n*=3 hearts], *Runx1*$^{wt/wt}$ MI [*n*=27 cardiomyocytes,*n*=4 hearts], *Runx1*$^{\Delta/\Delta}$ MI [*n*=23 cardiomyocytes,*n*=3 hearts]). **(L)** Ca^{2+} transients from cardiomyocytes transduced with Ad-GFP or Ad-Runx1. Mean: **(M)** Ca^{2+} transient peak; Ad-GFP (*n*=16 cardiomyocytes,*n*=6 hearts) and Ad-Runx1 (*n*=22 cardiomyocytes,*n*=6 hearts), **P*<0.05 linear mixed modelling **(N)** Caffeine-induced Ca^{2+} transient amplitude; Ad-GFP (*n*=13 cardiomyocytes,*n*=6 hearts) and Ad-Runx1 (*n*=19 cardiomyocytes,*n*=6 hearts), **P*<0.05 linear mixed modelling.

Figure 5. Phospholamban regulation in isolated cardiomyocytes from *Runx1*$^{\Delta/\Delta}$ mice 2 wk post-MI. (A) Western blot of phospholamban (PLB), phosphorylation of PLB at serine-16 [P-PLB (Ser16)] and pan-actin loading control. Percentage change in protein for **(B)** PLB and **(C)** P-PLB (Ser16/total PLB) (*Runx1*$^{\Delta/\Delta}$ MI [*n*=5 hearts] versus *Runx1*$^{wt/wt}$ and *Runx1*$^{fl/fl}$ MI [*n*=5 hearts]), **P*<0.05 Student's t-test. **(D)** Western blot of PKC, PLB, and PLB phosphorylation at threonine-17 (P-PLB (Thr17)). Percentage change in protein for **(E)** PKC and **(F)** P-PLB (Thr17/total PLB) (*Runx1*$^{\Delta/\Delta}$ MI [*n*=5 hearts] versus *Runx1*$^{wt/wt}$ MI and *Runx1*$^{fl/fl}$ MI [*n*=9 hearts]), **P*<0.05 Student's t-test. **(G)** Western blot of protein phosphatase 1 (PP1). **(H)** Percentage change in PP1 (*Runx1*$^{\Delta/\Delta}$ MI [*n*=5 hearts] versus *Runx1*$^{wt/wt}$ MI and *Runx1*$^{fl/fl}$ MI [*n*=9 hearts]). **(I, J, K)** Mean SERCA activity, caffeine–induced calcium transient amplitude and calcium transient amplitude data from Figure 4 compared to mean data obtained from 2 wk post-MI isolated cardiomyocytes with H89 (hatched white column; *Runx1*$^{wt/wt}$ MI and *Runx1*$^{fl/fl}$ MI+H89 [*n*=16 cardiomyocytes,3 hearts] and hatched red column; *Runx1*$^{\Delta/\Delta}$ MI+H89 [*n*=15 cardiomyocytes, 3 hearts]), **P*<0.05 Student's t-test.

Figure 6. *Runx1*$^{\Delta/\Delta}$ mice after ischemia with reperfusion (I/R). (A) Echocardiographic images (scale:x=0.1s;y=2mm). **(B)** Mean echocardiographic fractional shortening data of *Runx1*$^{fl/fl}$ I/R (*n*=9) and *Runx1*$^{\Delta/\Delta}$ I/R (*n*=8) [**P*<0.05], Student's t-test. **(C)** Mean infarct size (*Runx1*$^{fl/fl}$ I/R [*n*=9] and *Runx1*$^{\Delta/\Delta}$ I/R [*n*=7]), Student's t-test.

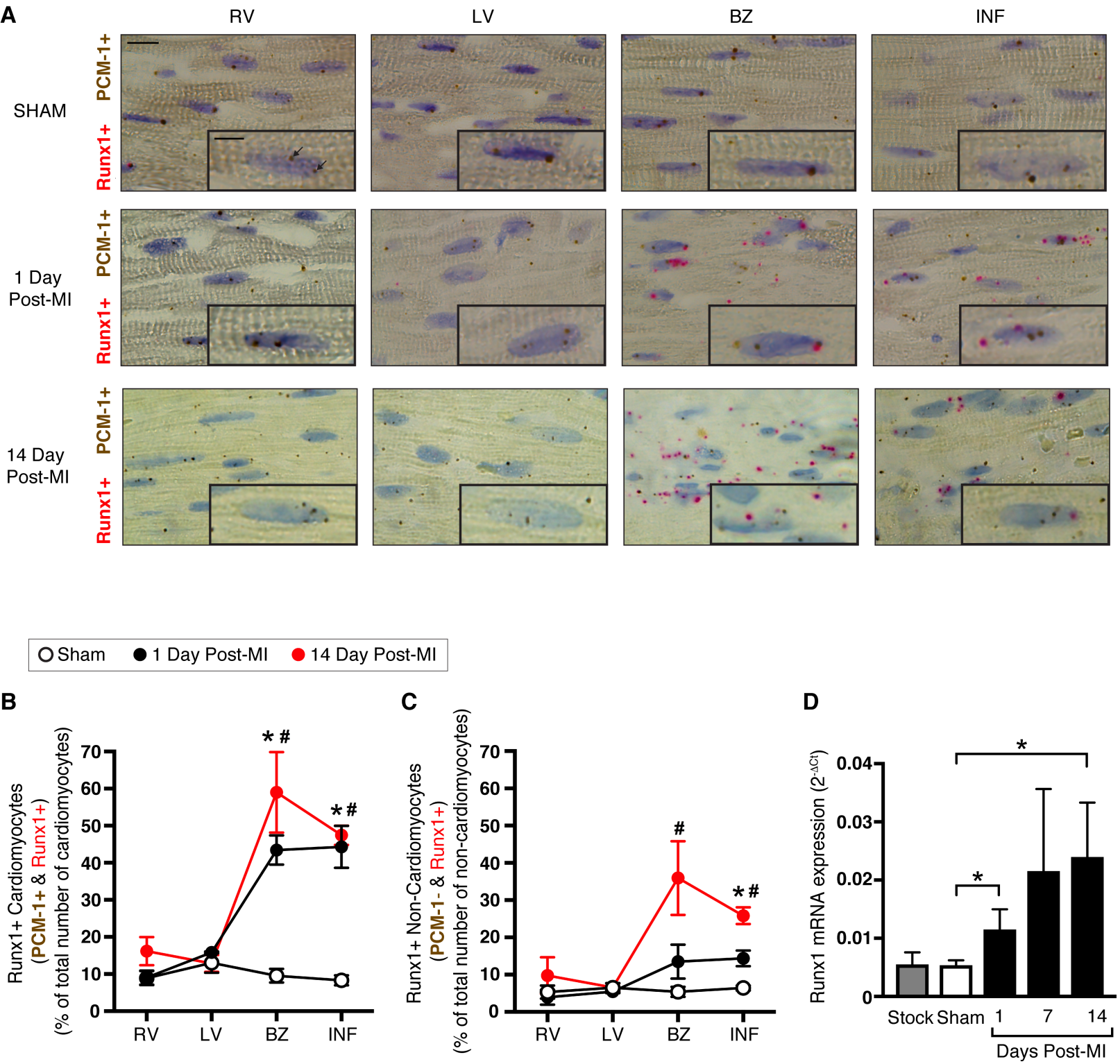
A
RV
LV
BZ
INF
SHAM
1 Day Post-MI
14 Day Post-MI
PCM-1+
Runx1+
Sham
1 Day Post-MI
14 Day Post-MI
B
Runx1+ Cardiomyocytes (PCM-1+ & Runx1+) (% of total number of cardiomyocytes)
C
Runx1+ Non-Cardiomyocytes (PCM-1- & Runx1+) (% of total number of non-cardiomyocytes)
D
Runx1 mRNA expression (2-ΔCt)
Stock
Sham
1
7
14
Days Post-MI

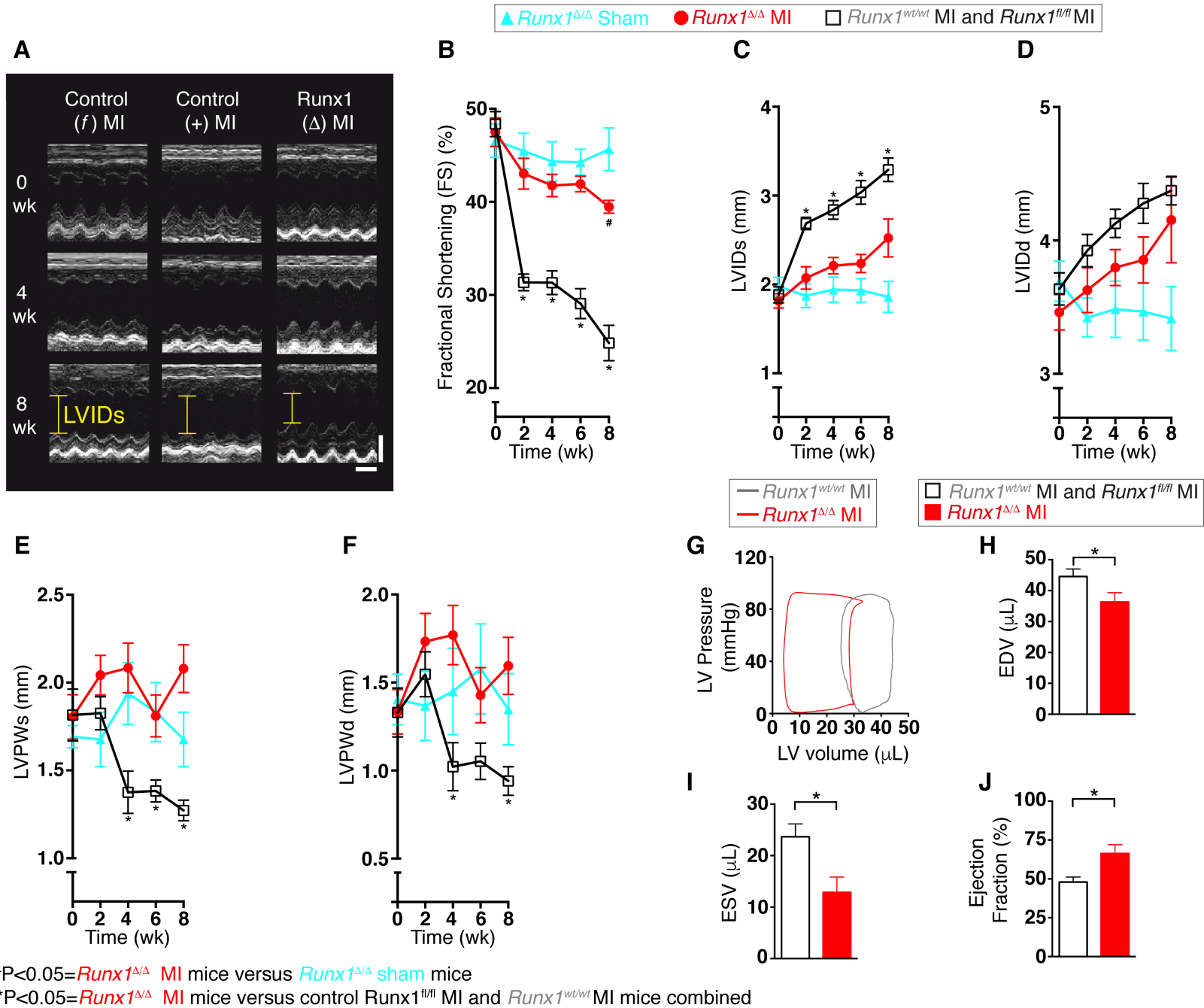

#P<0.05=*Runx1*$^{\Delta/\Delta}$ MI mice versus *Runx1*$^{\Delta/\Delta}$ sham mice

*P<0.05=*Runx1*$^{\Delta/\Delta}$ MI mice versus control Runx1$^{fl/fl}$ MI and *Runx1*$^{wt/wt}$ MI mice combined

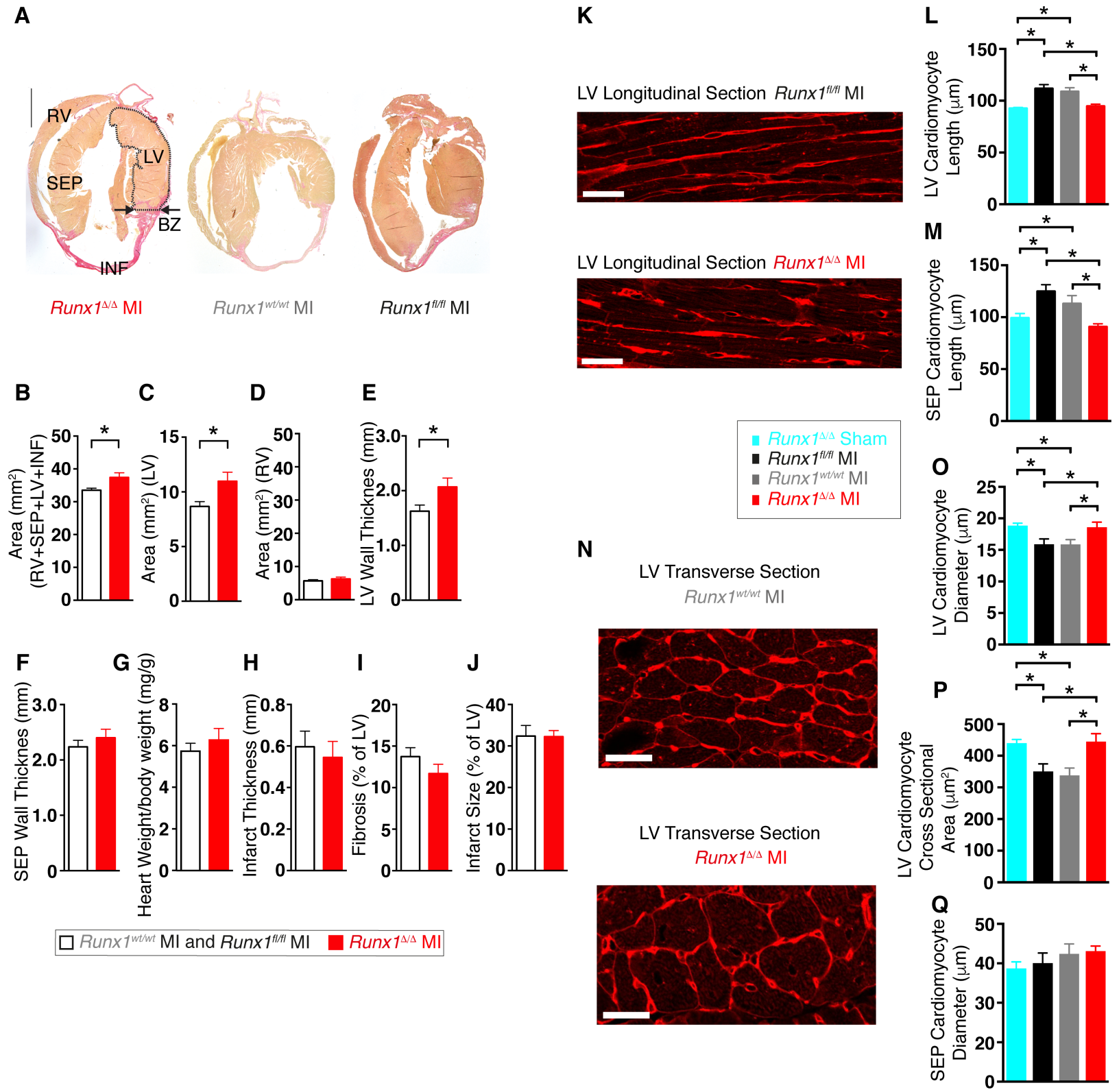
A
RV
LV
SEP
BZ
INF
Runx1Δ/Δ MI
Runx1wt/wt MI
Runx1fl/fl MI
B
Area (mm2) (RV+SEP+LV+INF)
C
Area (mm2) (LV)
D
Area (mm2) (RV)
E
LV Wall Thicknes (mm)
F
SEP Wall Thicknes (mm)
G
Heart Weight/body weight (mg/g)
H
Infarct Thickness (mm)
I
Fibrosis (% of LV)
J
Infarct Size (% of LV)
Runx1wt/wt MI and Runx1fl/fl MI
Runx1Δ/Δ MI
K
LV Longitudinal Section Runx1fl/fl MI
LV Longitudinal Section Runx1Δ/Δ MI
Runx1Δ/Δ Sham
Runx1fl/fl MI
Runx1wt/wt MI
Runx1Δ/Δ MI
N
LV Transverse Section
Runx1wt/wt MI
LV Transverse Section
Runx1Δ/Δ MI
L
LV Cardiomyocyte Length (μm)
M
SEP Cardiomyocyte Length (μm)
O
LV Cardiomyocyte Diameter (μm)
P
LV Cardiomyocyte Cross Sectional Area (μm2)
Q
SEP Cardiomyocyte Diameter (μm)

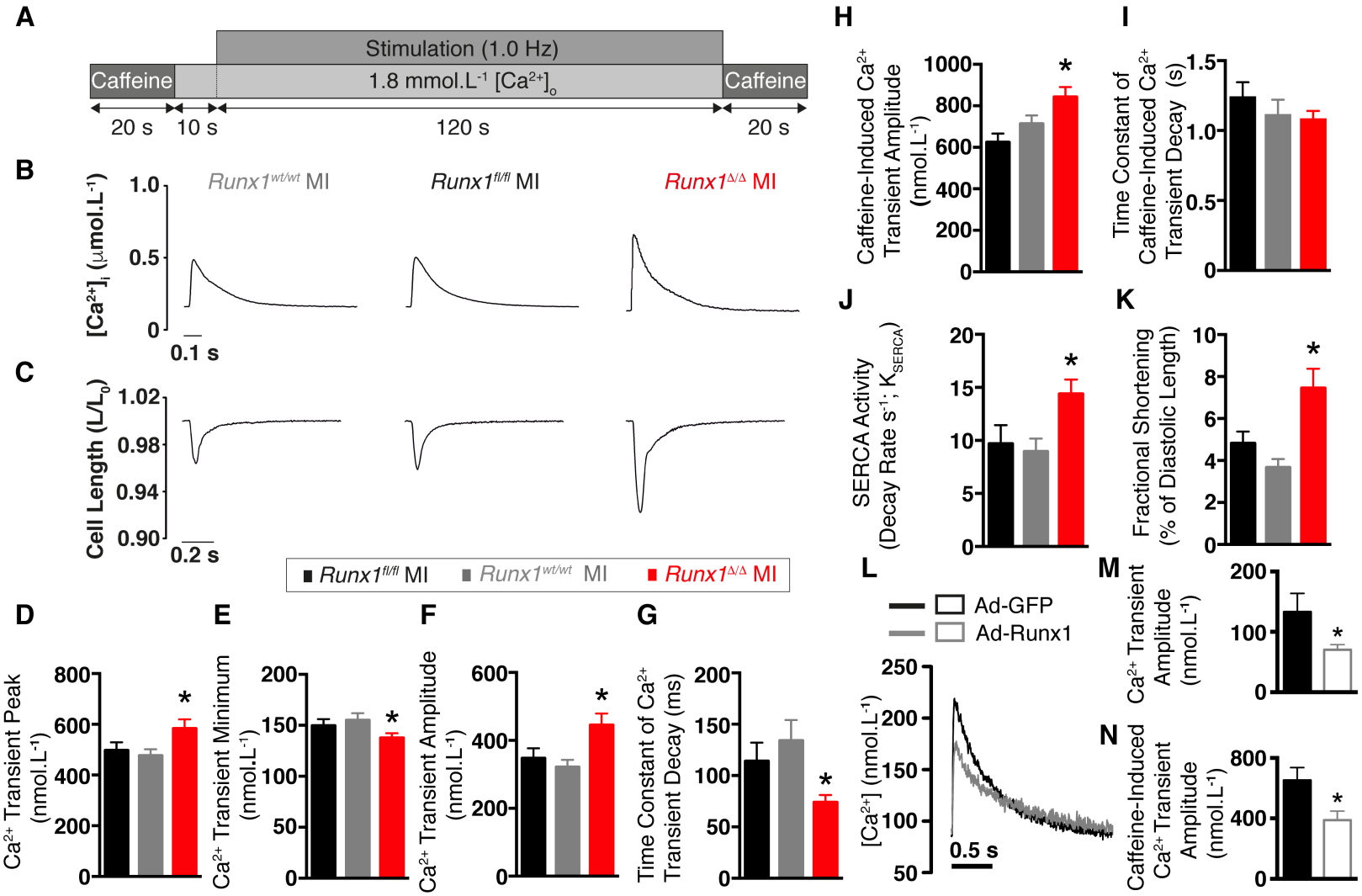
A
Stimulation (1.0 Hz)
Caffeine
1.8 mmol.L-1 [Ca2+]o
Caffeine
20 s
10 s
120 s
20 s
B
Runx1wt/wt MI
Runx1fl/fl MI
Runx1Δ/Δ MI
[Ca2+]i (μmol.L-1)
1.0
0.5
0
0.1 s
C
Cell Length (L/L0)
1.02
0.98
0.94
0.90
0.2 s
Runx1fl/fl MI
Runx1wt/wt MI
Runx1Δ/Δ MI
D
Ca2+ Transient Peak (nmol.L-1)
E
Ca2+ Transient Minimum (nmol.L-1)
F
Ca2+ Transient Amplitude (nmol.L-1)
G
Time Constant of Ca2+ Transient Decay (ms)
H
Caffeine-Induced Ca2+ Transient Amplitude (nmol.L-1)
I
Time Constant of Caffeine-Induced Ca2+ Transient Decay (s)
J
SERCA Activity (Decay Rate s-1; KSERCA)
K
Fractional Shortening (% of Diastolic Length)
L
Ad-GFP
Ad-Runx1
[Ca2+] (nmol.L-1)
0.5 s
M
Ca2+ Transient Amplitude (nmol.L-1)
N
Caffeine-Induced Ca2+ Transient Amplitude (nmol.L-1)

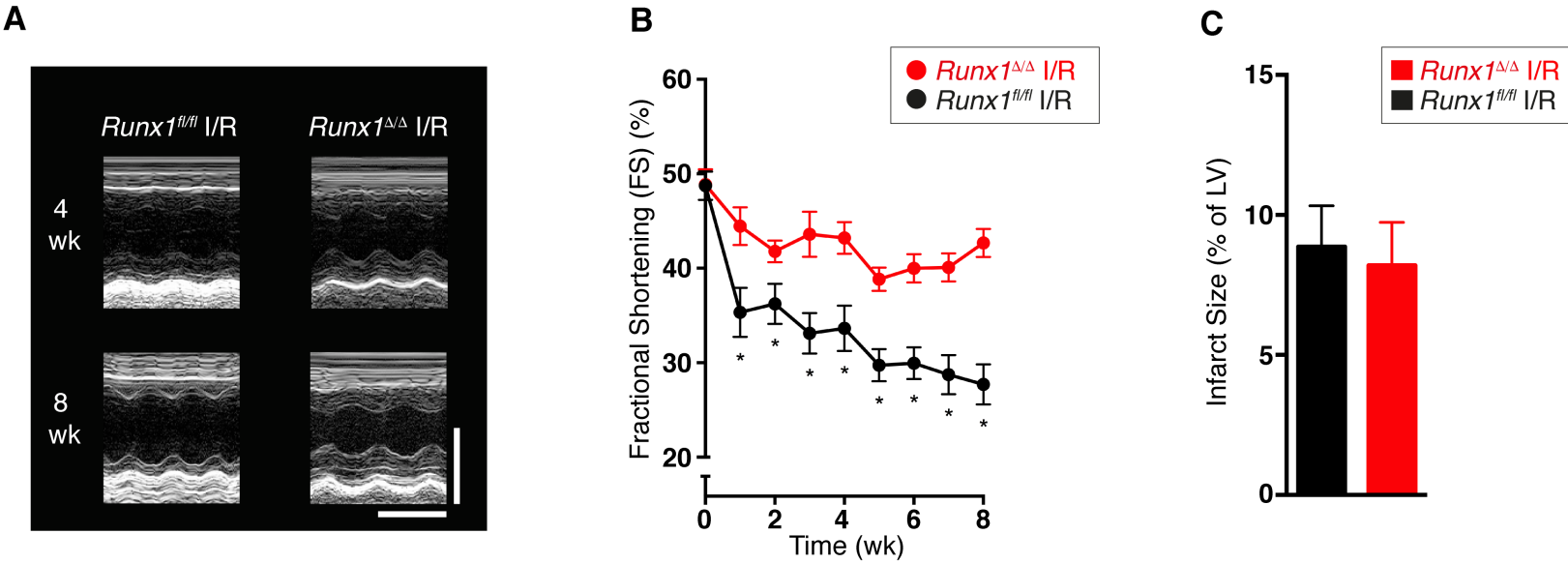
A
Runx1fl/fl I/R
Runx1Δ/Δ I/R
4 wk
8 wk
B
Runx1Δ/Δ I/R
Runx1fl/fl I/R
Fractional Shortening (FS) (%)
60
50
40
30
20
0
2
4
6
8
Time (wk)
C
Runx1Δ/Δ I/R
Runx1fl/fl I/R
Infarct Size (% of LV)
15
10
5
0

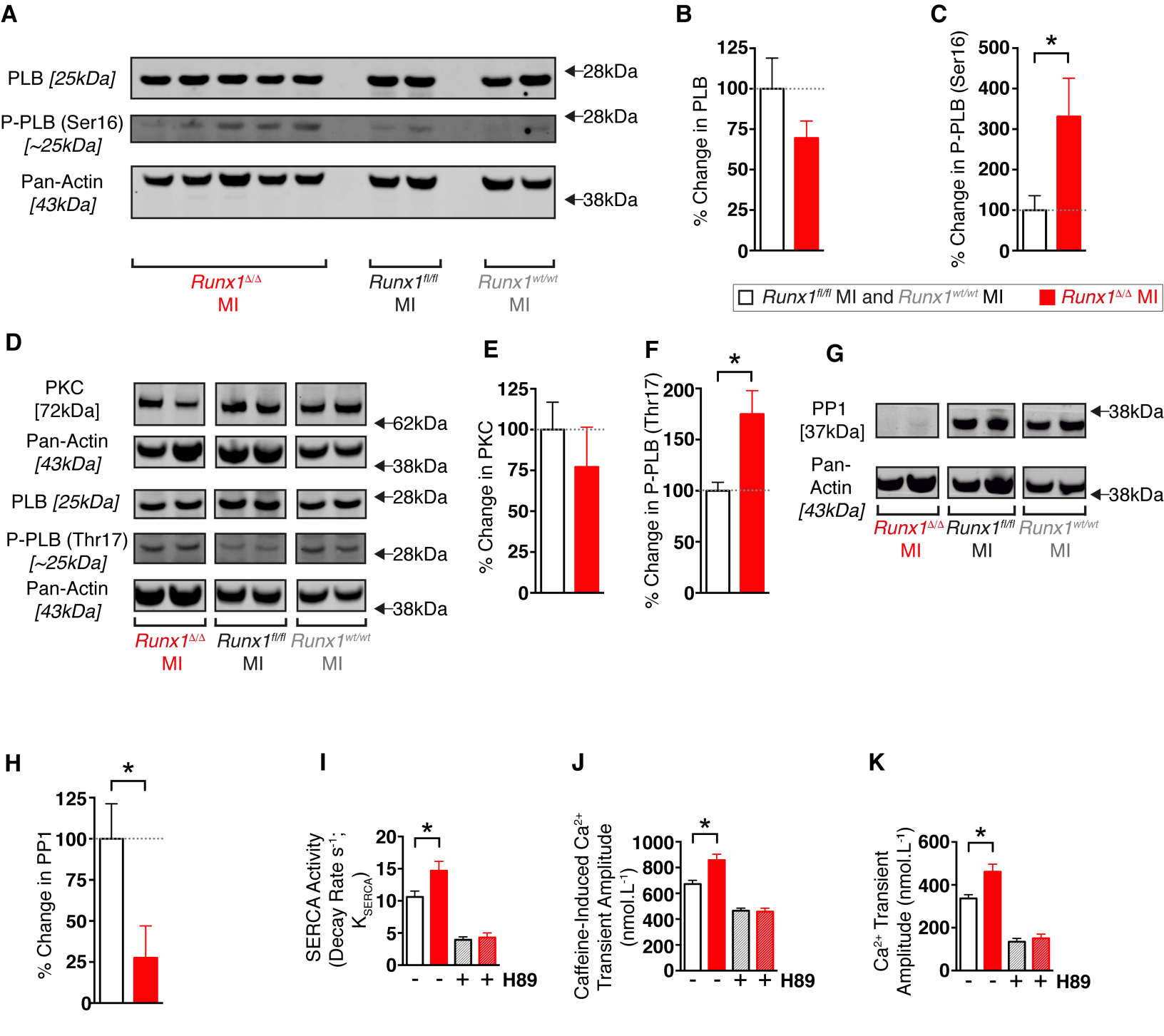
A
PLB [25kDa]
P-PLB (Ser16) [~25kDa]
Pan-Actin [43kDa]
28kDa
28kDa
38kDa
Runx1Δ/Δ MI
Runx1fl/fl MI
Runx1wt/wt MI
B
% Change in PLB
125
100
75
50
25
0
C
% Change in P-PLB (Ser16)
500
400
300
200
100
0
*
Runx1fl/fl MI and Runx1wt/wt MI
Runx1Δ/Δ MI
D
PKC [72kDa]
Pan-Actin [43kDa]
PLB [25kDa]
P-PLB (Thr17) [~25kDa]
Pan-Actin [43kDa]
62kDa
38kDa
28kDa
28kDa
38kDa
Runx1Δ/Δ MI
Runx1fl/fl MI
Runx1wt/wt MI
E
% Change in PKC
125
100
75
50
25
0
F
% Change in P-PLB (Thr17)
200
150
100
50
0
*
G
PP1 [37kDa]
Pan-Actin [43kDa]
38kDa
38kDa
Runx1Δ/Δ MI
Runx1fl/fl MI
Runx1wt/wt MI
H
% Change in PP1
125
100
75
50
25
0
*
I
SERCA Activity (Decay Rate s-1; KSERCA)
20
15
10
5
0
*
- - + + H89
J
Caffeine-Induced Ca2+ Transient Amplitude (nmol.L-1)
1000
800
600
400
200
0
*
- - + + H89
K
Ca2+ Transient Amplitude (nmol.L-1)
600
400
200
0
*
- - + + H89